Discover Electrochemistry

RESEARCH Open Access

A combined mechanical and fluid dynamic study of a medium power alkaline electrolyzer with prototype validation

David Levitán[1], Pedro Muñoz[2], Tomás Falaguerra[2], Victoria Benavente Llorente[3], Melisa J. Gomez[3], Gabriel Correa Perelmuter[3] and Esteban A. Franceschini[3*]

*Correspondence:
Esteban A. Franceschini
esteban.franceschini@mi.unc.edu.ar
[1]YPF Tecnología S.A., Av. del Petróleo Argentino 900-1198, 1925 Berisso, Buenos Aires, Argentina
[2]CREAS, Universidad Nacional de Catamarca - CONICET, Prado 366, K4700BDH, San Fernando del Valle de Catamarca, Catamarca, Argentina
[3]Dto. de Fisicoquímica - Facultad de Ciencias Químicas, INFIQC, Universidad Nacional de Córdoba - CONICET, Universidad Nacional de Córdoba, Ciudad Universitaria, 5000 Córdoba, Argentina

Abstract
This study presents the design, simulation, and experimental validation of a medium-power alkaline electrolyzer with a focus on structural, fluidics, and sealing performance. We evaluated the influence of electrode separator thickness on fluid dynamics and internal resistance, determining an optimal thickness of 3 mm. Mechanical simulations revealed that the structure remains intact under internal pressures of up to 15 bar, with acceptable stress distributions across all com- ponents. Fluidics tests demonstrated a uniform electrolyte distribution within the cells, ensuring optimal electrochemical performance. A two-cell stack was constructed as a prototype to validate sealing and flow behavior under realistic conditions. Hydraulic tests confirmed that the prototype maintained hermetic sealing at pressures up to 10 bar, with adjustments needed for 15 bar. Preliminary electrochemical testing using a KOH 30% wt. electrolyte confirmed stable oper- ation, although the cell voltage suggests that further optimization is required to reach high-performance benchmarks. Overall, the results highlight the robustness of the proposed design and its potential for future scale-up in green hydrogen production systems.

Keywords Hydrogen generation, Mechanical integrity, Fluid dynamics simulation, Electrochemical performance, Stack design, Prototype validation

1 Introduction

The global demand for sustainable energy solutions has led to a renewed interest in hydrogen production, particularly through water electrolysis [1–6]. As countries strive to reduce carbon emissions and transition towards renewable energy systems, hydrogen has emerged as a versatile and clean energy carrier with significant potential in various industrial applications. Among the available technologies, alkaline water electrolysis stands out due to its relatively low cost, mature technology, and scalability, making it a suitable candidate for large-scale hydrogen production [7, 8]. Recent advancements in materials science and engineering have facilitated the development of innovative

electrolyzer designs aimed at enhancing both efficiency and stability. However, achieving the ideal balance between mechanical integrity and fluid dynamics remains a challenge, particularly at elevated pressures and under varying operational conditions. Along with system temperature and electrode conditioning [9], factors such as separator thickness, material compatibility, and mechanical robustness are crucial in determining the overall performance and durability of the system [10–13].

This study focuses on the comprehensive design and analysis of a medium-power conventional alkaline electrolyzer, emphasizing mechanical stability, internal fluid dynamics, and electrochemical performance. Through a combination of computational fluid dynamics (CFD) simulations, finite element analysis (FEA), and real-world experimental validation, we aim to investigate the effects of separator thickness on fluid distribution, mechanical stresses under operational pressures, and overall system efficiency [12, 14, 15]. By integrating theoretical and practical approaches, we aim to establish a robust framework for evaluating the interplay between structural stability and electrochemical efficiency. In addition, we assess the influence of different separator materials and configurations to determine their impact on gas management and pressure distribution within the electrolyzer cell.

The findings from this research will contribute to the optimization of alkaline electrolyzers, ultimately supporting the development of robust and efficient systems for hydrogen production. In addition to evaluating electrochemical performance, this study also addresses critical challenges associated with scalability and long-term durability, focusing on material degradation and component resilience under prolonged use. Developing electrolyzers capable of withstanding harsh operational environments while maintaining high efficiency is essential for their widespread adoption.

Furthermore, this work aligns with national and international efforts to promote renewable energy technologies, contributing to the global agenda for decarbonization and sustainable energy transition. By exploring innovative designs and materials, this study seeks to provide valuable insights that enhance the performance and reliability of alkaline electrolyzers, paving the way for their integration into future energy infrastructures. Ultimately, the outcomes of this research are expected to offer prac-tical guidelines for industrial applications, focusing on achieving higher performance metrics while minimizing operational risks and costs. In this work, we present a detailed analysis of the design, construction, and performance evaluation of a medium- power alkaline electrolyzer, aiming to achieve mechanical stability while addressing key challenges related to fluid dynamics and durability.

2 Prototype design

The aim is to design an electrolyzer capable of operating with an energy consumption of around 10 kW, using approximately 20 cells, each running at 0.5 A cm^{-2}. The goal is to produce around 2 $Nm^3\ h^{-1}$ of hydrogen at 10 bar pressure, with 30% wt. KOH as the electrolyte. Zirfon UTP 500 + membranes will be used as diaphragms to main- tain gas separation, and it is essential to keep the cathodic and anodic electrolytes separate to prevent gas mixing and enhance product quality [16]. The electrodes will consist of electrochemically nickel-plated AISI316L stainless steel with a thickness of 0.7 mm, and polypropylene spacers will be used between the electrodes, offering good thermal and chemical resistance. Although this configuration provides a suitable platform for initial

testing, it is acknowledged that Ni-based materials offer limited catalytic activity, particularly at the anode [17, 18]. Future iterations of the design will incorporate more active anodic coatings to enhance oxygen evolution reaction (OER) performance. In addition, while the current planar plate configuration does not implement a true zero-gap design, it does offer structural compatibility with such configurations. In fact, nickel-plated steel sheets are commonly employed as mechanical and electrical supports for porous electrodes, such as nickel foams, in zero-gap architectures. Therefore, once tightness and pressure resistance are ensured, this structure could be relatively easily adapted into a zero-gap electrolyzer with improved electrochemical performance. The thickness of the electrode spacers will be analyzed to minimize ohmic resistance by reducing the gap between electrodes as much as possible, while avoiding bubble accumulation inside the cell caused by confinement at the electrodes. At this initial stage, 500 μm thick commercial PTFE gaskets will be used to ensure the prototypes' tightness at various pressures. AISI316L stainless steel end plates with a thickness of 22 mm will be used, secured with 12 M8 bolts, to distribute pressure evenly over the gaskets, ensuring internal and external tightness and preventing gas mixing or leakage. Given the operational parameters, a single cell operating at 3 V and 0.5 A cm^{-2} (according to a very conservative approach), with 20 cells in total, requires an active electrode area of 310 cm^2 to achieve a power output of approximately 9 kW (9300 W theoretical) with a theoretical hydrogen production of 2 Nm^3/h^{-1}. A cell of this size would operate at a total current of 155 A and a potential of approximately 60 V. Fig. S1 presents a schematic of a bipolar electrolyzer, illustrating the electrical connections and the electrolyte flow circuit.

2.1 Mesh selection

Automatic meshing tools from SOLIDWORKS® were used for the studies. Three different mesh densities were tested, and halving the element size resulted in only a 3.7% variation in the results at a 15 bar inner pressure and 18,500 N·m torque in the washers, confirming mesh stability. Therefore, the selected mesh provided an adequate balance between computational cost and accuracy for the flow dynamics simulations. In contrast, for the mechanical simulation studies, a curvature-based dense mesh was applied, following the parameters specified in Table 1. The mesh was automatically generated based on the geometry and guided by the internal quality criterion of SOLIDWORKS® [19, 20] (Fig. S2):

Table 1 Mesh parameters

Parameter	Value
Mesh type	Solid mesh
Type of mesh algorithm	Curvature based mesh
Jacobian points	4 points
Max element size	20.8 mm
Min element size	4.2 mm
Element type	Quadratic high order elements
Nodes	85,133
Elements	39,080
Max aspect ratio	102.91
Element fraction with aspect ratio < 3	45.5
Element fraction with aspect ratio > 10	22.5
Fraction of distorted elements (Jacobian)	0

3 Results

3.1 Cell design

Having established the geometry of the electrode spacers and considering that the active area needs to be approximately 310 cm^2, the design of the electrodes and gaskets was initiated to ensure proper cell assembly and guarantee its tightness. For this purpose, 316L nickel-plated steel electrodes with a total thickness of 0.7 mm were selected, cut to match the channel geometry corresponding to the nozzles. Although this design introduces the issue of shunt currents on the electrodes (Fig. S4), particularly near the nozzle area, these currents are expected to be minimal. This electrode geometry facilitates the tightness of the cell gasket, reducing the number of parts compared to a design that would use, for instance, insulating frames to support the electrodes. The gaskets, made of 0.5 mm thickness PTFE film, have two main geometries: one located at the contact between the electrode and the electrode spacer (Fig. 1a–d), which essentially outlines the active area and surrounds the entire electrode to prevent gas leaks and electrolyte mixing near the nozzle area. There are also gaskets designed to hold the Zirfon membrane in place (Fig. 1b), preventing it from shifting and causing electrolyte mixing in this region. In this case, the property of Zirfon to act as a gasket is also leveraged [21, 22]. Additionally, initial and final gaskets are intended to isolate the end plates, i.e., the anode and cathode electrodes, to prevent them from facing each other and causing gas mixing. Figure 1 presents the initial gasket, the gaskets corresponding to the electrode and Zirfon, and the final cell gasket. At this point, having established the materials and geometry of the cell, the effect of the electrode spacer thickness was analyzed, as it has a direct impact on the liquid layer thickness. Subsequently, an analysis of the cell's tightness, deformation of gaskets, spacers, end plates, and Zirfon was conducted to study the load distribution, resistance to internal pressure, etc., ensuring no parts fall below the safety factor determined by the yield strength of the materials used (Sect. 3.4). To facilitate the understanding of the cell architecture, Fig. S5 presents an exploded view of the two-cell alkaline electrolyzer, detailing the arrangement of all components, including end plates, gaskets, electrode separators, diaphragms, and electrodes. This schematic allows a clear visualization of the internal configuration and sealing interfaces within the stack, complementing the subsequent mechanical and fluidics analyses.

3.2 Internal fluidics simulation

An initial cell design was created using the parameters mentioned in the previous section, considering 3 mm electrode spacers. The goal was to optimize the internal fluid dynamics of the electrolyzer, maximizing the active electrode area and avoiding zones

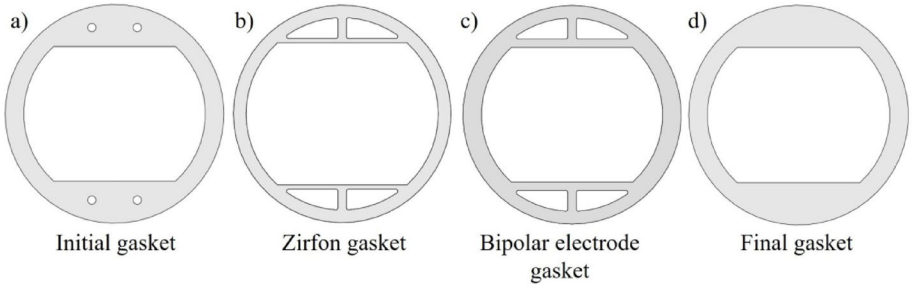

Fig. 1 Schematic sketch of the different PTFE gaskets used in the design

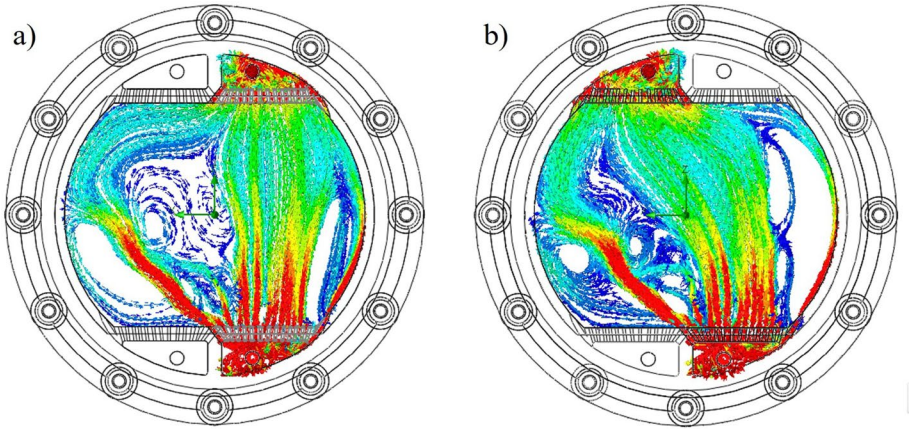

Fig. 2 Diagrams of the electrolyte supply and distribution system. **a** vertical flow. **b**: diagonal flow.

Table 2 Electrolyte properties (KOH 30% wt.) at 298 K and 1 bar [24]

Parameter	Value
Density/kg m^{-3}	1290
Dynamic visc./Pa s	0.0018
Specific heat/J kg^{-1} K^{-1}	3250
Thermal conductivity/W m^{-1} K^{-1}	0.55
Flow rate /L min^{-1}	15

of low electrolyte circulation (circulation exclusion zones), which could generate bubble accumulation [23] and lead to inefficient use of the catalysts.

As this is a bipolar electrolyzer, the goal is for the electrode spacers to guide the electrolyte flow to optimize electrode utilization. A diagonal flow of electrolyte is established, in contrast to a vertical flow, with electrolyte entering through the lower nozzles and exiting, mixed with gases, through the upper nozzles. This design aims to minimize zones where electrolyte circulation is blocked.

Figure 2 shows examples of circulation exclusion zones when using either a vertical or diagonal electrolyte flow. A flow simulation was conducted using the parameters shown in Table 2):

Figure 2 shows the results of the flow simulations, considering electrolyte input from lower nozzles and output from upper nozzles, focusing only on the cathodic channel. In Fig. 2a the vertical flow is depicted, while Fig. 2b shows the configuration for diagonal flow. To assess the improvement in electrode utilization when using vertically or diagonally positioned nozzles, the electrolyte velocity on the electrode surface was established as the enhancement parameter.

Electrolyte velocities below 0.025 m s^{-1} were considered low, indicating under utilization of the electrode. This threshold was established based on the work of Balzer and Vogt [25], who reported that below this velocity, bubble coverage on gas-evolving electrodes becomes stable due to insufficient forced convection, leading to limited surface cleaning and reduced active area. Therefore, the flow distribution for both configurations was analyzed to determine the areas of the electrode with electrolyte velocities below this threshold. This threshold was chosen as a representative low flow velocity to highlight regions of poor circulation; although the value is arbitrary, it provides a practical basis for comparing flow uniformity across different inlet configurations.

In the vertical flow configuration, low-flow regions covered approximately 40% of the electrode, reducing efficiency. The diagonal flow, while not fully optimizing electrode utilization, improved electrolyte distribution. Specifically, vertical nozzles resulted in 38.8% of the electrode surface experiencing low velocities, whereas diagonal nozzles reduced this to 33.7%, improving utilization by 5%.

Further improvements could potentially be achieved by exploring different types of nozzles or electrolyte distributors in future designs.

3.3 Effect of electrolyte layer thickness

In this context, computational simulations were conducted with different thicknesses of electrode spacers, which determine the thickness of the liquid layer where the electrochemical reaction takes place. Electrode spacers with thicknesses of 3, 7 and 10 mm were tested [26]. Fluidics simulations were repeated to identify low-velocity zones in the electrolyte, with the aim of determining whether increasing the thickness of the electrode spacers reduces dead zones in the electrolyzer by decreasing electrolyte confinement. It was found that a 3 mm spacer does not significantly differ from 7 or 10 mm spacers in terms of fluid dynamics, and there are no major improvements from increasing the spacer thickness. However, a decrease in system efficiency was observed when increasing the spacer thickness due to a rise in over-voltage as the distance between the electrodes increases. Therefore, we selected a 3 mm electrode spacer thickness as the optimal choice based on the conditions considered for this cell.

3.4 Mechanical simulation method

At present, there is a wide variety of software available to analyze and simulate real engineering problems, commonly known as Computer-Aided Engineering (CAE) [27, 28]. The stress and strain distribution of the system can be obtained using this type of software. SolidWorks Simulation is the SOLIDWORKS® module that solves these problems through the application of the Finite Element Method (FEM). FEM is a numerical technique used to find approximate solutions to partial differential equations within a system. The system is divided into many subsystems, producing a mesh. These subsystems are called finite elements, and each element has a determined number of nodes where the partial differential equation is solved. The mechanical properties of the materials used for the simulation are presented in Table 3.

In Fig. S3, an example of the bipolar cell structure subjected to compression is presented, aimed at determining whether the materials can withstand the stress they will encounter to achieve tightness at different pressures, reaching a maximum of 15 bar while considering an operating pressure of 10 bar. Forces were applied to the different washers of the support bolts. The washers on one side were fixed to the geometry to serve as an anchor for the entire model, while the washers on the opposite side were

Table 3 Mechanical properties of the materials proposed for the stack construction

	Teflon	Polypropylene	AISI 316L (SS)	Zirfon®
Elastic modulus/N m^{-2}	550.0	1408.5	2.00×10^{5}	310.0
Poisson coef./1	0.4	0.4	0.3	0.4
Density/kg m^{-3}	2200	900	7850	1000
Shear limit/N m^{-2}	7.58	33	580	–
Elastic limit/N m^{-2}	24.52	29.42	172.37	8.00
Thermal expansion coef./K	1.22×10^{-4}	1.80×10^{-3}	1.21×10^{-5}	6.90×10^{-5}

subjected to a force of 12.500 N (equivalent to a torque of 20 N m per unit), which should ensure tightness at 10 bar. This experiment is conducted to determine if the different components will maintain their integrity at this torque under ambient pressure. A static study was performed to determine the stress distribution, strain and displacements in the various components of the prototype. After analyzing these parameters, the components were examined for areas that fell below the established safety factor (defined as 1.5 times the ratio of maximum expected compressive stress to material strength in compression).

In Fig. 3, the results of the accumulated stresses in the end plate are presented. It is observed that the highest stress concentration occurs at the washers where compression forces are applied. In the end plate (Fig. 3a and b), the stress distribution is quite homogeneous; although there is a higher concentration in the outer zones, no sufficiently high stress accumulation is detected that could lead to undesired defor- mation. Analyzing the edges of the end plate, it is noted that the movable plate, i.e., the one where the torques are applied, shows greater deformation than the back plate, which contains the fixed washers. However, the accumulated stresses are acceptable for a prototype of this scale.

In the analysis of the electrode spacers, it is observed that the accumulated stresses are low (Fig. 3c and d).

Regarding the gaskets, both those containing the Zirfon and those of the electrodes show acceptable accumulated stresses, which are within the expected range for a gasket that must deform to ensure the sealing. Additionally, the accumulated stress in the Zirfon and its respective gasket is similar, suggesting that the Zirfon could also partially function as a gasket (Fig. 3e).

The accumulated stresses in the electrodes are low enough to rule out problems related to sealing or potential dangerous deformation (Fig. 3f). The inhomogeneous stress pattern observed in the electrode area is attributed to the aspect ratio of the plates and the fact that the compressive force is applied primarily at the edges, which allows a slight flexing in the central region. Finally, in the areas connecting the electrolyte channels to the active zone, an increase in accumulated stress is noticeable, though within acceptable values, without implying significant deformations that could pose a problem (Fig. 3g).

In Fig. S6, images corresponding to the safety factor in terms of pass/fail are presented. The blue areas correspond to where the deformation is below the safety factor (1.5 times the maximum expected compressive stress), while the red areas indicate where it would not be acceptable. Thus, all components of the stack are within the safety factor, and no rupture issues are expected.

These analyses were performed at ambient pressure of one atmosphere, considering electrode spacers with thicknesses of 3, 7 and 10 mm. In all cases, the accumulated stresses were sufficiently low to not represent a design problem, allowing for further studies of internal fluid dynamics with each of the considered electrode spacers, keeping in mind that from an electrochemical perspective, a thinner electrode spacer is desirable, as it reduces the ohmic drop by shortening the ionic path between electrodes [29, 30]. However, excessively thin gaps may induce electrolyte confinement and promote the formation of low-flow regions, particularly in flat plate geometries, leading to bubble accumulation and reduced effective electrode area. Conversely, increasing the spacer thickness can alleviate these fluid dynamic limitations by enabling more uniform

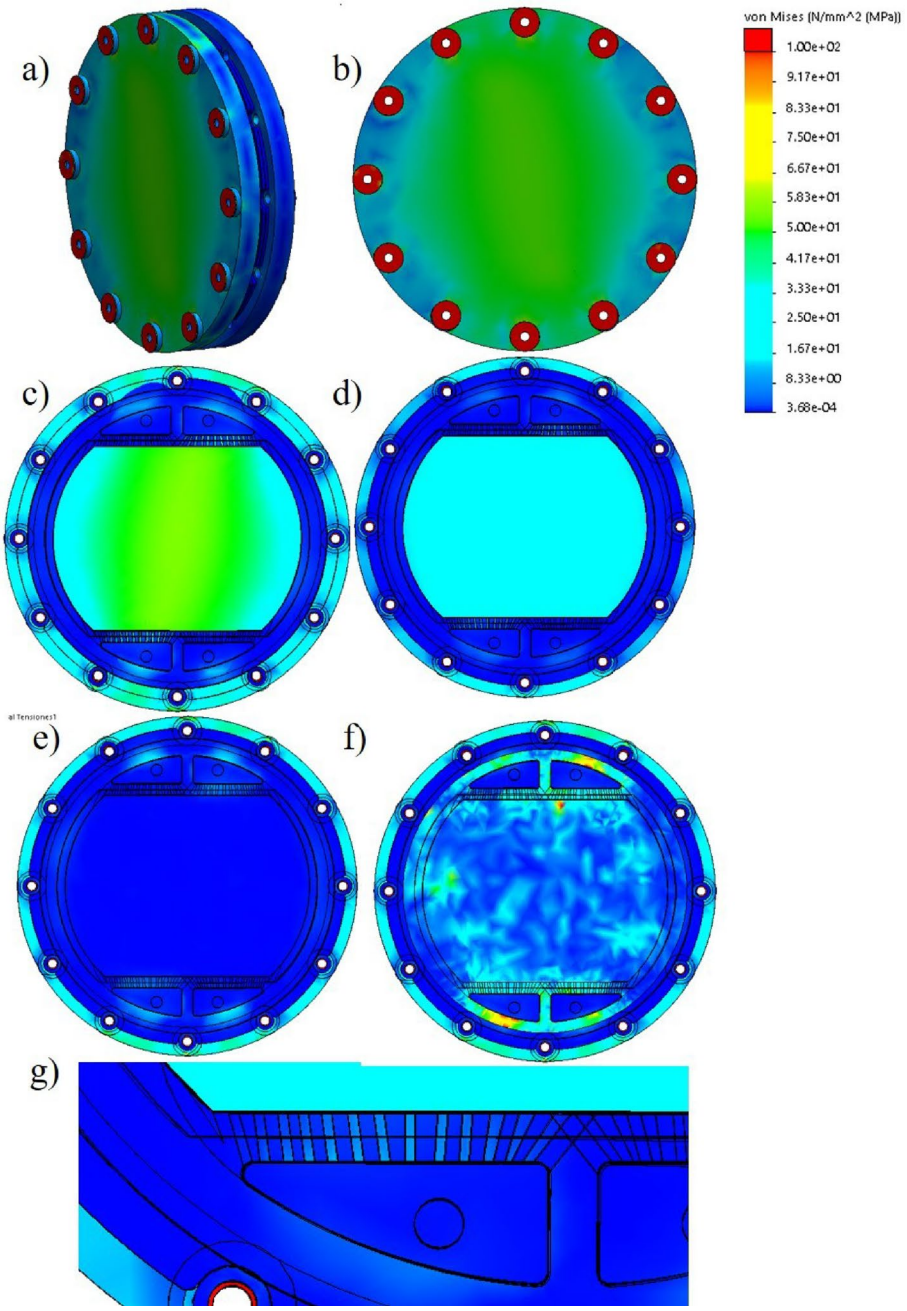

Fig. 3 Results of the accumulated stresses in: **a** and **b** complete cell, **c** electrode gasket, **d** electrode separator, **e** Zirfon and Zirfon gasket, **f** electrode and **g** mag-nification of the channel region in the 3 mm thick electrode separator

electrolyte circulation [26], even though it comes at the cost of higher ohmic resistance. Having established that there would be no substantial improvement by increasing the thickness of the electrode separators, an optimal thickness of 3 mm was defined for conducting mechanical stability simulations at 15 bar of internal pressure, comparing it with that obtained at ambient pressure (presented in Sect. 3.4).

3.5 Mechanical simulation under internal pressure

Mechanical simulations were performed by applying an internal pressure of 10 bar and a force on the bolts of 12 500 N (equivalent to a torque of 20 N m) per bolt. In Fig. 4a, mesh used in the simulation is shown, along with the distribution of internal (red arrows) and external forces (green and orange arrows) corresponding to the applied torque to support the assembled system and the applied internal pressure.

It was found that an internal pressure of 10 bar does not have a substantial effect on the cell structure, and similar to what is observed when the cell is subjected to ambient pressure, all components are below the established safety factor (Fig. 4b). A new mechanical simulation was performed using the SolidWorks simulation package to analyze an internal pressure of 15 bar, seeking to establish how the prototype behaves within an overpressure condition of 1.5 times the operating pressure for which it was designed (10 bar). To achieve this, it was necessary to increase the torque on the screws to obtain a force of 18750 N per screw (equivalent to 30 N m of torque). This was because at lower torques, the system was not stable, possibly due to the internal pressure exceeding the supporting force. Although it was reported again that all components are below the safety factor, it is important to analyze the possibility of deformation in the different parts that make up the cell.

To analyze the results obtained from this simulation, a cross-sectional cut was made to study the deformation of the various parts. In particular, deformation of the electrode separators was found due to the internal pressure, where the internal plates expand approximately 2.5 mm in radius (over a total piece radius of 125 mm). This expansion, while acceptable from a mechanical standpoint, would generate small misalignments that could affect the internal fluid dynamics of the cell. Although a radial displacement of approximately 2.5 mm over a 125 mm radius may appear significant, this corresponds to a deformation of only 2%, which is well below the failure strain of polypropylene. According to Da Costa et al. [31], the elongation at break for polypropylene can reach values as high as 150%, with typical failure strains above 15%, depending on processing and crystallinity. Therefore, the observed deformation is entirely within the elastic regime for the material, and no plastic deformation or functional compromise is expected under the tested conditions. Furthermore, the pro- totype maintained

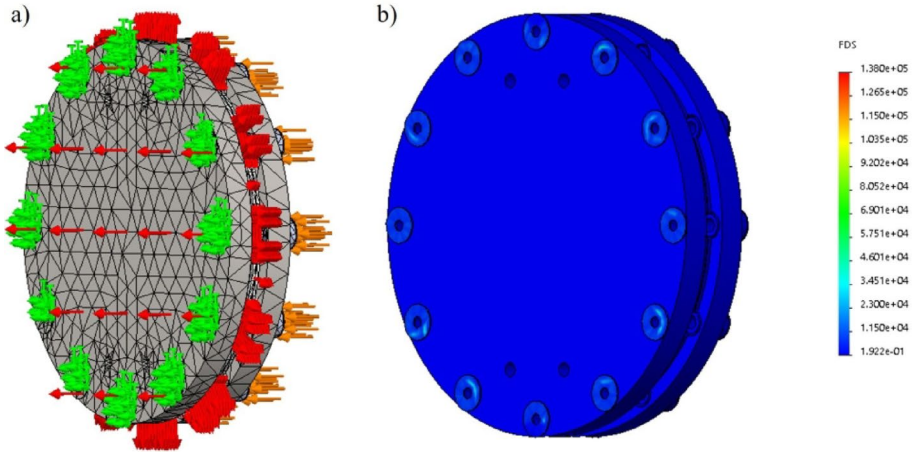

Fig. 4 **a** Mesh used in the simulation and the distribution of(red arrows) and external forces (green and orange arrows) corresponding to the applied torque and internal pressure. **b** Security factor of the complete two-cell stack

mechanical integrity and sealing up to 15 bar of internal pressure. In Fig. 5, a cross-section of the cell is presented, focusing on the edge where the displacement of the electrode separators is observed when an internal pressure of 15 bar is applied.

3.6 Fluidics testing of a 20-cells stack at ambient pressure

To conduct a study of the internal fluidics of the different electrolyzers, a model of the stack with 20 cells was developed. The Flow Simulation package from SOLIDWORKS® was used to simulate the input of 15 L min^{-1} of 30% wt. KOH electrolyte at ambient temperature. With the aim of obtanining a uniform intake of electrolyte among the cells, the distribution was studied in the domains of the stack model. Flow was analyzed within the nozzles, in the active area, and in the entrance to each cell. A fluidic study was performed with the parameters found in Table 2 for density, dynamic viscosity, flow rate, etc., and the results are presented in Figs. 6 and 7. Figure 6a shows the longitudinal section of the inlet nozzles, where the velocity distribution is observed. It is found that, while there is a higher circulation velocity at the center, aligned with the connection to the external pipe, the liquid collides with the end electrode and redistributes within the nozzle. Figure 6b and c illustrate how the electrolyte enters the cell through each of the rectangular channels leading to the active area. It can be seen that, although there are some differences in the velocities of the different inlet channels to each cell and in the distribution of velocities between cells, these differences are not significant. The electrolyte is expected to be distributed in a sufficiently homogeneous manner across the 20 cells comprising the stack.

It is important to clarify that this simulation does not take into account bubble formation or accumulation; it only considers the movement of the electrolyte.

The pressure drop across the 20 cell stack was found to be 6.2 for this simulation. This result is in the order of magnitude of comparable electrochemical flat-plate cell stacks [32] as well as alkaline electrolyzer system simulation results [33].

The internal fluidics experiments were repeated for electrode separators with thicknesses of 7 and 10 mm, and no substantial improvement was found in the internal fluidics of the cells or in the velocity distribution. Therefore, it is considered that the 3 mm

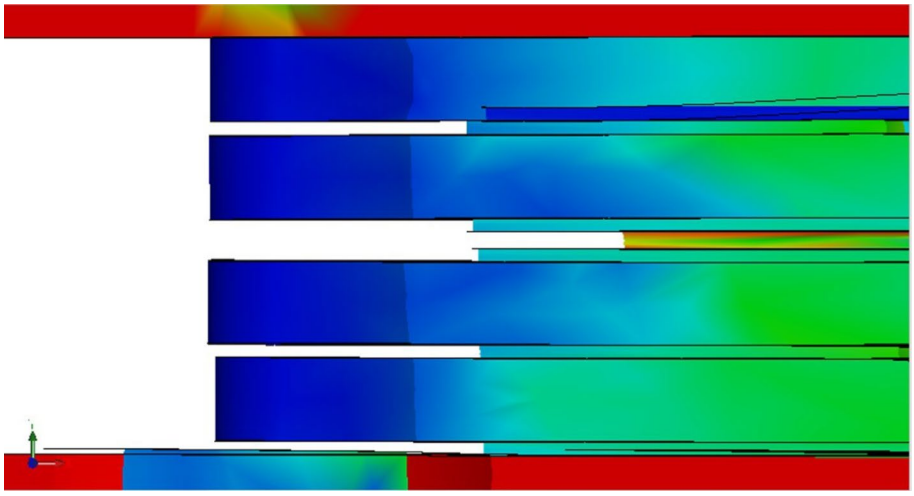

Fig. 5 Cross-section of the cell showing the displacement of the electrode separators under an internal pressure of 15 bar

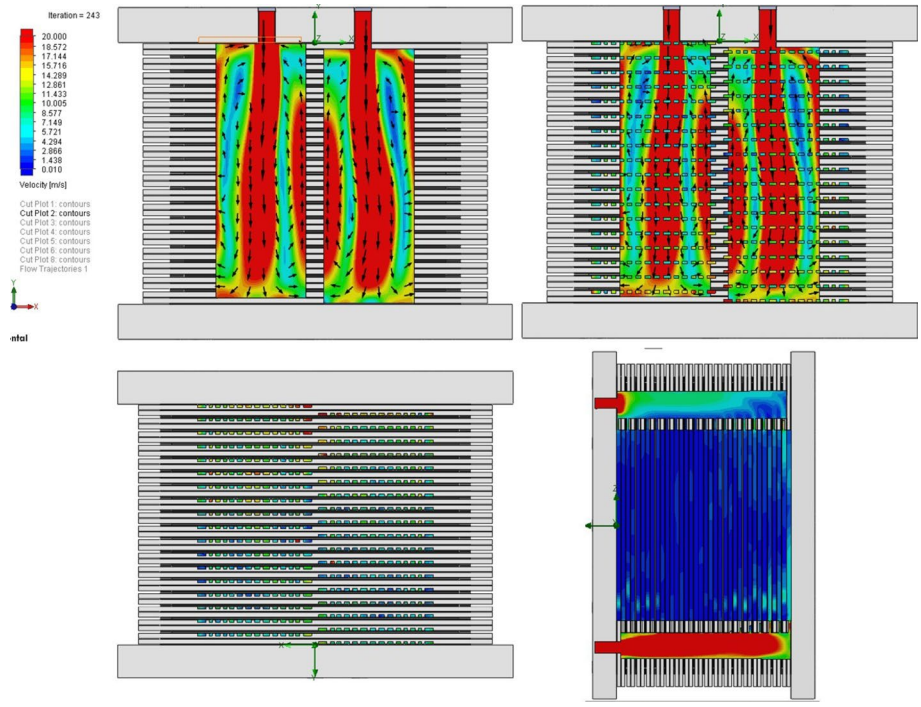

Fig. 6 Results of the internal fluid dynamics study, showing the electrolyte velocity distribution in the inlet nozzles and rectangular channels using 3 mm thick electrode separators

thick separators are appropriate from a fluid dynamics perspective. Furthermore, reducing separator thickness minimizes the ohmic drop of the cell [29, 34], and thus the 3 mm separator is selected for the construction of the prototype.

Figures 7 and S7 (the latter provided as a video in the supplementary information) present, respectively, a static image and a video illustrating the particle analysis (flow trajectories), showing the distribution and movement of the electrolyte within each cell. In the video, the particle motion is clearly observed, with higher velocities at the inlet and outlet manifolds and relatively lower velocities within the cells, highlighting the flow patterns.

4 Prototype construction

The construction of the two-cell stack prototype was carried out using the materials presented in Table 3. AISI316L stainless steel was used for the end plate, with a diameter of 30 cm and a thickness of 22 mm. The AISI 316L sheets have a thickness of 0.7 mm, laser-cut and coated with a layer of 40 μm thick electrolytic nickel [35, 36]. Teflon sheets of 0.5 mm thickness were used to create the gaskets, and Zirfon Pearl 500 + sheets served as diaphragm membranes. Finally, homopolymer polypropylene plates of 3 mm thickness were used to machine the electrode separators.

Figure 8b presents a photograph of the assembled two-cell prototype, which was used to perform hydraulic tests evaluating the sealing integrity under various bolt torque conditions. It was determined that a torque of 20 N m maintained sealing integrity at internal pressures up to 10 bar without leakage; however, at an internal pressure of 15 bar, this torque was insufficient, requiring an increase in the applied bolt torque to ensure tightness. Figure 8c shows the constructed cell along with a polariza- tion curve obtained using a 30% wt. KOH electrolyte, a flow rate of 2.2 L min^{-1}, and applying

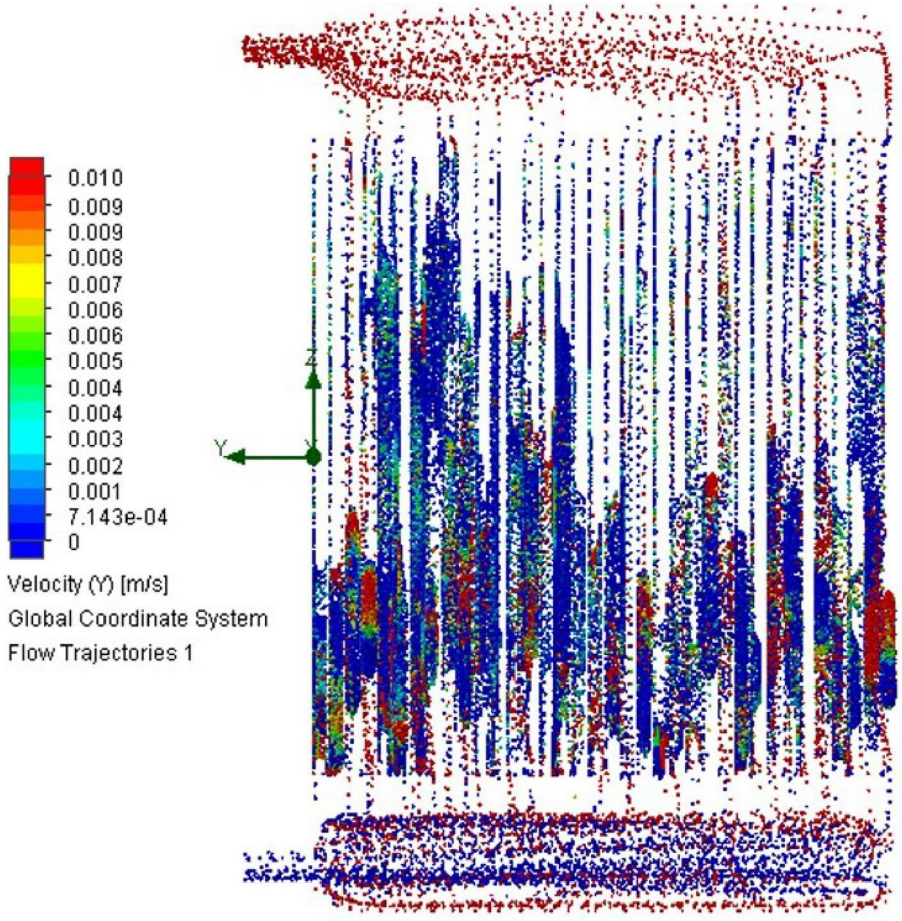

Fig. 7 Particle analysis (flow trajectories) indicating the flow of electrolyte within each cell of the stack

current steps during 300 s to stabilize the potential. These measure- ments were performed at room temperature and ambient pressure to determine the proper functioning of the cell. If we compare the obtained polarization curve with the state-of-the-art values for conventional alkaline electrolyzers obtained from the litera- ture [37, 38], we found an acceptable response with a potential of 2.67 V at 0.52 A cm^{-2} per cell. Although the cell potential is higher than expected, it can be improved by an electrode conditioning process, stacking, temperature increase, etc. which enables further experimental optimization. The proper conditioning of the cell stack ensures a lower potential during operation, as well as a more stable energy consumption. The reader is referred to a recently published work for further details [39].

5 Conclusions

In this work, we presented a comprehensive study of the mechanical design, fluid dynamics, and experimental evaluation of a conventional alkaline electrolyzer. The integration of advanced simulation techniques and experimental validation allowed us to optimize the geometry and operating conditions of the electrolyzer, leading to significant improvements in performance and efficiency.

Our design approach focused on minimizing ohmic resistance and enhancing electrolyte management through precise electrode spacing and optimized flow distribution.

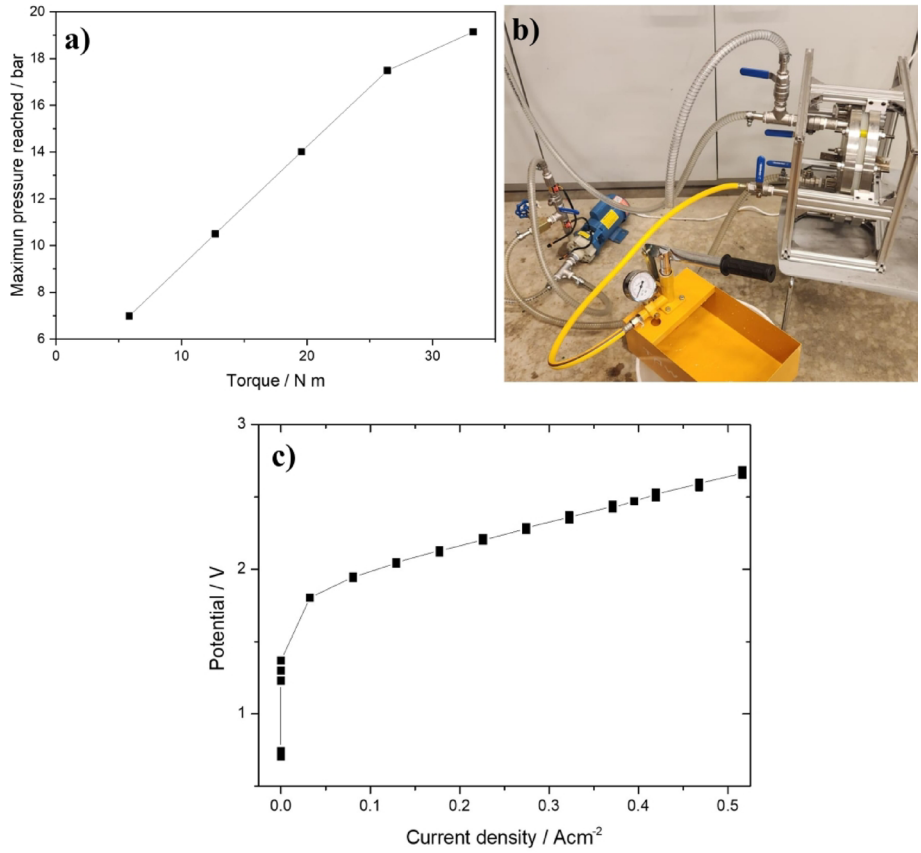

Fig. 8 **a** Maximum pressure reached at different bolt tightening torques. **b** Photo-graph of the assembled two-cell stack for hydraulic tests at different bolt tightening torques. **c** Polarization curve obtained from the two-cell stack built according to the design developed in this work, measured at an electrolyte flow rate of 2.2 L per minute with current steps of 0.05 A·cm^{-2}.Potential is shown per cell

Diagonal nozzle configuration improved utilization by 5% with respect to vertical nozzle configuration. The optimal electrode spacing was found to be 3 mm. A low pressure drop of 6.2 was calculated for a 20 cell stack.. The fluid dynamic simulations demonstrated that the proposed configuration effectively produced uniform flow patterns across the electrode surface, as well as across the different cells within the stack. This led to an improved gas–liquid interface, enhancing the overall electrochemical performance.

Mechanically, the proposed design was studied by simulation under the rated pressure of 10 bar, showing structural integrity and no noticeable deformation for an applied torque of 20 N m. The design was further studied under an overpressure condition of 15 bar, where deformations in the elastic regime were observed for the separators, and sealing was maintained for the stack for an applied torque of 30 N m. Experimentally, the electrolyzer prototype demonstrated an acceptable power con- sumption of 2.67 V at 0.52 A cm^{-2} current density, showing stable operation during polarization measurements. The results indicated that the developed prototype show- cases robustness and reliability under various operating conditions, highlighting its potential for large-scale hydrogen production applications.

Future work will focus on further scaling the technology and integrating additional control strategies to maximize efficiency. Additionally, ongoing efforts will be directed toward evaluating long-term durability and developing advanced diagnostic tools to

monitor in situ performance. The knowledge gained from this study contributes significantly to the development of next-generation alkaline electrolyzers for sustainable hydrogen production.

Supplementary Information

The online version contains supplementary material available at https://doi.org/10.1007/s44373-025-00076-0.

Supplementary file 1.

Supplementary file 2.

Acknowledgements
MG thanks CONICET for her postdoctoral fellowship. DL thanks CONICET and YTEC for his postdoctoral fellowship. PM, TF, VB, GCP and EAF are permanent research fellows of CONICET.

Author contribution
D.L. performed the modelling and design work in SolidWorks. E.F., G.C., and M.G. conceived the original design concept and proposed modifications. E.F., V.B., and G.C. provided funding through research projects. D.L., T.F., and P.M. conducted the experimental measurements for validation. E.F., D.L., and P.M. wrote the original manuscript draft. All authors reviewed and approved the final version of the manuscript.

Funding
This research was funded by Agencia Nacional de Promoción Científica y Tecnológica (ANPCyT PICT 2019–0856), COFECYT (CB-05/PFI-2021 and CB-3-PFI-2022) and CONICET (PIP 179025).

Data availability
The data generated during this study are stored in the institutional repository of CONICET and are available upon reasonable request to the corresponding author. https://ri.conicet.gov.ar/

Declarations

Ethics approval and consent to participate
Not applicable.

Consent for publication
Not applicable.

Competing interests
The authors declare no competing interests.

Received: 25 July 2025 / Accepted: 28 November 2025
Published online: 06 December 2025

References

1. International Energy Agency: Global Hydrogen Review 2023. Technical report, International Energy Agency (2023). https://www.iea.org/reports/ global-hydrogen-review-2023
2. Shiva Kumar S, Lim H. An overview of water electrolysis technologies for green hydrogen production. Energy Rep. 2022;8:13793–813. https://doi.org/10.1016/j.egyr.2022.10.127.
3. Nnabuife SG, Hamzat AK, Whidborne J, Kuang B, Jenkins KW. Integra-tion of renewable energy sources in tandem with electrolysis: a technology review for green hydrogen production. Int J Hydrogen Energy. 2024. https://doi.org/10.1016/j.ijhydene.2024.06.342.
4. Shaya N, Glöser-Chahoud S. A review of life cycle assessment (LCA) stud-ies for hydrogen production technologies through water electrolysis: recent advances. Energies. 2024. https://doi.org/10.3390/en17163968.
5. Hassan NS, Jalil AA, Rajendran S, Khusnun NF, Bahari MB, Johari A, et al. Recent review and evaluation of green hydro- gen production via water electrolysis for a sustainable and clean energy society. Int J Hydrogen Energy. 2024;52:420–41. https://doi.org/10.1016/j.ijhydene.2023.09.068.
6. Cavaliere P. Water electrolysis for hydrogen production. Water Electrol Hydrogen Prod. 2023. https://doi.org/10.1007/978-3-031-37780-8.
7. Ehlers JC, Feidenhans'l AA, Therkildsen KT, Larrazábal GO. Affordable green hydrogen from alkaline water electrolysis: key research needs from an industrial perspective. ACS Energy Lett. 2023;8(3):1502–9. https://doi.org/10.1021/acsenergylett.2c02897.
8. Olabi AG, bahri A, Abdelghafar AA, Baroutaji A, Sayed ET, Alami AH, et al. Large-vscale hydrogen production and storage technologies: Current status and future directions. Int J Hydrogen Energy. 2021;46(45):23498–528. https://doi.org/10.1016/j.ijhydene.2020.10.110.
9. Appelhaus S, Ritz L, Pape SV, Lohmann-Richters F, Kraglund MR, Jensen JO, et al. Benchmarking performance: a round-robin testing for liquid alkaline electrolysis. Int J Hydrogen Energy. 2024;95:1004–10. https://doi.org/10.1016/J.IJHYDENE.2024.11.288.

10. Groot MT, Vreman AW. Ohmic resistance in zero gap alkaline electrolysis with a Zirfon diaphragm. Electrochim Acta. 2021;369:137684. https://doi.org/10.1016/j.electacta.2020.137684.
11. Faqeeh AH, Symes MD. Zero-gap bipolar membrane water electrolyzers: prin-ciples, challenges and practical insights. Electrochim Acta. 2024;493:144345. https://doi.org/10.1016/j.electacta.2024.144345.
12. Gavrailov D, Ibrahim N, Boycheva S. Improved alkaline electrode configuration and CFD modeling comparison between different electrolysers. In2024 5th International conference on communications, information, electronic and energy systems (CIEES) 2024 Nov 20 (pp. 1–6). IEEE.
13. Santos AL, Cebola M-J, Santos DMF. Towards the hydrogen econ-omy—a review of the parameters that influence the efficiency of alkaline water electrolyzers. Energies. 2021. https://doi.org/10.3390/en14113193.
14. Hess S, Zhang S, Kadyk T, Galkina I, Beale SB, Eikerling M, et al. Multi-scale computational fluid dynamics simulation of alkaline water elec-trolyzers: A numerical investigation. ECS Meeting Abstracts. 2024. https://doi.org/10.1149/MA2024-02463287mtgabs.
15. Muhsen H, Alshawabkeh M, Al-Mahmodi M, Ghanem A, Al-Halhouli A. Sensitivity analysis of electrodes spacing media for evaluating alkaline electrolyzer performance through CFD modeling. Renew Energy Focus. 2024;49:100575. https://doi.org/10.1016/j.ref.2024.100575.
16. Choi BB, Jo JH, Lee T, Jeon S-Y, Kim J, Yoo Y-S. Operational characteristics of high-performance kW class alkaline electrolyzer stack for green hydrogen production. J Electrochem Sci Technol. 2021;12(3):302–7. https://doi.org/10.33961/jecst.2021.00031.
17. Colli AN, Girault HH, Battistel A. Non-precious electrodes for practical alkaline water electrolysis. Materials. 2019;12(8):1336. https://doi.org/10.3390/ma12081336.
18. Li T, Liu W, Xin H, Sha Q, Xu H, Kuang Y, et al. Large-scale and simple synthesis of NiFe(OH)x electrode derived from Raney Ni precursor for efficient alkaline water electrolyzer. Catalysts. 2024;14(5):296. https://doi.org/10.3390/catal14050296.
19. Salmat S, Yanti Sari D, Fernanda Y, Prasetya F. SolidWorks flow simu-lation: selecting the optimal mesh for conducting CFD analysis on a centrifugal fan. J Eng Res Lect. 2023;2(3):94–103. https://doi.org/10.58712/jerel.v2i3.104.
20. Sabin M. Criteria for comparison of automatic mesh generation methods. Adv Eng Softw Work. 1991;13(5):220–5. https://doi.org/10.1016/0961-3552(91)90028-3.
21. Vermeiren P, Adriansens W, Leysen R. Zirfon®: a new separator for Ni-H2 batteries and alkaline fuel cells. Int J Hydrogen Energy. 1996;21(8):679–84. https://doi.org/10.1016/0360-3199(95)00132-8.
22. Hickmann T. Gasket solutions for electrolyzers—an overview. Int J Res. 2023;11(5):57–61. https://doi.org/10.29121/granthaalayahv11.i5.2023.5183.
23. Grigoriev SA, Porembskiy VI, Korobtsev SV, Fateev VN, Auprêtre F, Millet P. High-pressure PEM water electrolysis and corresponding safety issues. Int J Hydrogen Energy. 2011;36(3):2721. https://doi.org/10.1016/j.ijhydene.2010.03.058.
24. Haynes WM. CRC handbook of chemistry and physics. London: CRC Press; 2016.
25. Vogt H, Balzer RJ. The bubble coverage of gas-evolving electrodes in stagnant electrolytes. Electrochim Acta. 2005;50(10):2073–9. https://doi.org/10.1016/J.ELECTACTA.2004.09.025.
26. Lavorante MJ, Reynoso CY, Franco JI. Straight-parallel electrodes and variable gap for hydrogen and oxygen evolution reactions. Int J Electrochem. 2019;2019(1):5392452. https://doi.org/10.1155/2019/5392452.
27. Kurowski, P.M.: Engineering Analysis with SolidWorks Simulation 2019. SDC Publications, Mission, KS (2019). https://www.sdcpublications.com/Textbooks/Engineering-Analysis-SOLIDWORKSSimulation
28. Magomedov IA, Sebaeva ZS. Comparative study of finite element analysis software packages. J Phys Conf Ser. 2020;1515(3):32073. https://doi.org/10.1088/1742-6596/1515/3/032073.
29. Opu MS. Effect of operating parameters on performance of alkaline water electrolysis. Int J Therm Environment Eng. 2015;9(2):53–60. https://doi.org/10.5383/ijtee.09.02.001.
30. Gomez M, Levitan D, Muñoz P, Falaguerra T, Longinotti MP, Humana T, et al. Unveiling OER bubble dynamics in alkaline electrolysis: impacts on cell resistance. Int J Hydrogen Energy. 2025;106:138–45. https://doi.org/10.1016/J.IJHYDENE.2025.01.263.
31. Da Costa HM, Ramos VD, Rocha MCG. Rheological properties of polypropylene during multiple extrusion. Polym Test. 2005;24(1):86–93. https://doi.org/10.1016/J.POLYMERTESTING.2004.06.006.
32. Bjareklint A, Carlsson L, Sandegren B Design of SU modular-ized electrochemical cells. Am Inst Chem Eng Nat Meeting (1983)
33. Qi R, Becker M, Brauns J, Turek T, Lin J, Song Y. Channel design optimization of alkaline electrolysis stacks considering the trade-off between cur-rent efficiency and pressure drop. J Power Sources. 2023;579:233222. https://doi.org/10.1016/J.JPOWSOUR.2023.233222.
34. Okonkwo PC, Bhowmik H, Mansir IB, Al MA, Al Sfarini NF. Effect of electrode spacing on hydrogen production using a home-made alkaline electrolyzer. Mater Lett. 2022;1(306):130841. https://doi.org/10.1016/J.MATLET.2021.130841.
35. Gomez MJ, Franceschini EA, Lacconi GI. Ni and NixCoyAlloys elec- trodeposited on stainless steel AISI 316L for hydrogen evolution reaction. Electrocatalysis. 2018;9(4):459–70. https://doi.org/10.1007/s12678-018-0463-5.
36. Gómez MJ, Lucci RO, Franceschini EA, Lacconi GI. Effect of TiO_2 content on Ni/TiO_2 composites electrodeposited on SS316L for hydrogen evolu-tion reaction. Electrochim Acta. 2021;378:138136. https://doi.org/10.1016/jelectacta.2021.138136.
37. Schalenbach M, Tjarks G, Carmo M, Lueke W, Mueller M, Stolten D. Acidic or alkaline? Towards a new perspective on the efficiency of water elec- trolysis. J Electrochem Soc. 2016;163(11):3197. https://doi.org/10.1149/2.0271611jes.
38. Ju W, Heinz MV, Pusterla L, Hofer M, Fumey B, Castiglioni R, et al. Lab-scale alkaline water electrolyzer for bridging material fundamentals with realistic operation. ACS Sustain Chem Eng. 2018;6(4):4829–37.
39. Muñoz P, Falagüerra T, Gomez M, Llorente VB, Levitán D, Franceschini E, et al. Conditioning and testing of a medium-power alkaline electrolyzer stack at high current densities for green hydrogen production. Int J Hydrogen Energy. 2025;5(165):150731.

Publisher's Note